

High magnetic field induced crossover from the Kondo to Fermi liquid behavior in $1T$ -VTe₂ single crystals

Xiaxin Ding^{1,2,*}, Jie Xing², Gang Li³, Luis Balicas³, Krzysztof Gofryk¹, and Hai-Hu Wen²

¹*Idaho National Laboratory, Idaho Falls, Idaho, 83402, USA.*

²*Center for Superconducting Physics and Materials,
National Laboratory of Solid State Microstructures and Department
of Physics, Nanjing University, Nanjing 210093, China and*

³*National High Magnetic Field Laboratory, Florida State University, Tallahassee-FL 32310, USA*

The magnetic and magnetotransport properties of metallic $1T$ -VTe₂ single crystals were investigated at temperatures from 1.3 to 300 K and in magnetic fields up to 35 T. Upon applying a high magnetic field, it is found that the electrical resistivity displays a crossover from the logarithmic divergence of the single-impurity Kondo effect to the Fermi liquid behavior at low temperatures. The Brillouin scale of the negative magnetoresistivity above the Kondo temperature $T_K = 12$ K indicates that the Kondo features originate from intercalated V ions, with $S = 1/2$. Both magnetic susceptibility and Hall effect show an anomaly around T_K . By using the modified Hamann expression we successfully describe the temperature-dependent resistivity under various magnetic fields, which shows the characteristic peak below T_K due to the splitting of the Kondo resonance.

I. INTRODUCTION

Layered transition metal dichalcogenides (TMDCs) have attracted enormous attention because they exhibit a rich variety of physical properties and a striking potential for applications [1–3]. The wide range of transport properties of bulk TMDCs varies from conventional superconductivity [4] via charge density wave (CDW) [5] to exceedingly large positive magnetoresistivity (MR) [6] at low temperatures. Furthermore, layered TMDCs are easily intercalated with metallic ions due to their layered structures [7]. For example, Cu intercalated TiSe₂ exhibits a CDW to superconducting transition upon doping [8]. When magnetic $3d$ transition metals (Co, Ni and Fe) are intercalated into TiSe₂, the Kondo effect is induced in the dilute limit [9]. Similarly, the Kondo effect has been reported in bulk VSe₂, probably due to the interlayer V ions [10]. In addition, TMDCs are ideal for studying the interplay between electronic properties and crystalline dimensionality. With the development of exfoliation and epitaxial techniques, monolayered TMDCs could be successfully produced demonstrating distinct properties from their bulk counterparts. In contrast to paramagnetism in bulk VSe₂, ferromagnetism is observed in monolayer VSe₂ at room temperature [11]. In monolayer VTe₂, which is isostructural to VSe₂, the suppression of a CDW transition is a matter of debate [12–15]. In bulk VTe₂, a CDW transition occurs upon cooling across 480 K, which is accompanied by a structural phase transition from the high-temperature trigonal phase ($1T$ structure) to the low-temperature monoclinic phase [16–19]. Using the vapor transport method, the single crystalline VTe₂ has a monoclinic structure corresponding to the low-temperature polymorph [20]. By contrast, high-temperature polymorph $1T$ -VTe₂ single crystals can be

successfully grown via the molten-salt method. Furthermore, this reveals characteristics of the Kondo effect at low temperatures [21], which was later found in $1T$ -VTe₂ nanoplates [22].

In this manuscript, we study the evolution of the Kondo effect under high magnetic fields in $1T$ -VTe₂ single crystals. The Kondo effect, discovered in 1930 by Meissner and Voigt [23] and then explained by Kondo in 1964 [24], has recently generated recently renewed interest due to progress in nanotechnology [25, 26]. In condensed matter physics, it also provides clues to allow understanding of the electronic properties of various strange metals, such as superconductors and heavy-fermion materials. The spin-exchange process between localized impurities and itinerant electrons of the metallic host generates a new state at the Fermi level, known as the Kondo resonance or Abrikosov-Suhl resonance peak [27]. The first hint of this new state manifests itself as an anomalous upturn in the resistivity below the Kondo temperature T_K , which is the energy scale dependent on spin-exchange coupling and limiting the validity of the Kondo effect. Specifically, the temperature-dependent resistivity $\rho(T)$ of the Kondo system shows the approximate logarithmic increase with decreasing temperature in a small range below T_K and T^2 Fermi liquid behavior for $T \ll T_K$. Moreover, the splitting of the Kondo resonance under the applied magnetic field correlates with a characteristic peak in the temperature and magnetic field dependence of the resistivity $\rho(T, B)$. These transport properties for a single Kondo impurity can be calculated by a nonperturbative approach, such as the numerical renormalization group (NRG) method [28, 29]. However, despite all of these advances, the lack of a systematic understanding remains on the low-temperature behavior of the electrical resistivity, especially in the presence of high magnetic fields [30].

Here, we systematically study the transport and magnetic properties of $1T$ -VTe₂ single crystals under high magnetic fields. The temperature and magnetic field de-

* xiaxin.ding@inl.gov

pendence of the magnetization, resistivity, and Hall effect reveal Kondo effect characteristics with $T_K = 12$ K. Both magnetic susceptibility and MR measurements determined that the local magnetic moments arise from the intercalated V ions with $S = 1/2$. The characteristic peaks in $\rho(T, B)$ are observed below T_K and can be analyzed by a modified Hamann expression. By applying a magnetic field up to 35 T, the Kondo effect is gradually suppressed, and the Fermi liquid behavior emerges at low temperatures.

II. EXPERIMENTAL DETAILS

$1T$ - VTe_2 single crystals were grown by the flux method using KCl as the flux. First, we prepared the polycrystalline samples by a solid-state reaction method, with V powders (purity 99.5%, Alfa Aesar) and Te grains (purity 99.5%, Alfa Aesar) in the ratio of 1 : 2. The mixture was compressed into a pellet, then loaded into an alumina crucible and sealed in an evacuated quartz tube, subsequently heated up to 750 °C for 20 h. Second, powders with a molar ratio of $KCl : VTe_2 = 4 : 1$ were heated up to 950 °C for 2 days, followed by cooling down to 800 °C at a rate of 1 °C/h. Finally, we obtained single crystals with lateral sizes of 2-4 mm and thickness of about 10-50 μm by dissolving the flux in deionized water. The samples are stable in water and display silver color. All the weighing, mixing, grinding and pressing procedures were finished in a glovebox under Ar atmosphere. X-ray diffraction (XRD) measurements were performed using a Bruker D8 Advanced diffractometer with Cu K_α radiation. The energy dispersive X-ray (EDX) spectrum measurements were performed on a scanning electron microscope under an accelerating voltage of 20 kV (Hitachi Co., Ltd.). The magnetization measurements were carried out using a SQUID-VSM-7T Quantum Design device. The small enhancement, around 50 K in the temperature dependence of the magnetic susceptibility at 1 T, is induced by an antiferromagnetic transition due to a small amount of solid oxygen in the measurement chamber. Electrical transport measurements were done in a Quantum Design PPMS-16T instrument using a standard four-probe method, with the electrical current applied along the plane of samples. The high field MR was measured at the National High Magnetic Field Laboratory in Tallahassee.

III. RESULTS AND DISCUSSION

A. X-ray diffraction

The XRD pattern of the as-grown $1T$ - VTe_2 single crystals at room temperature is shown in Fig. 1. Similar to its sister compounds [18, 31–33], our VTe_2 single crystals display a trigonal CdI_2 -type structure ($1T$ phase) with V

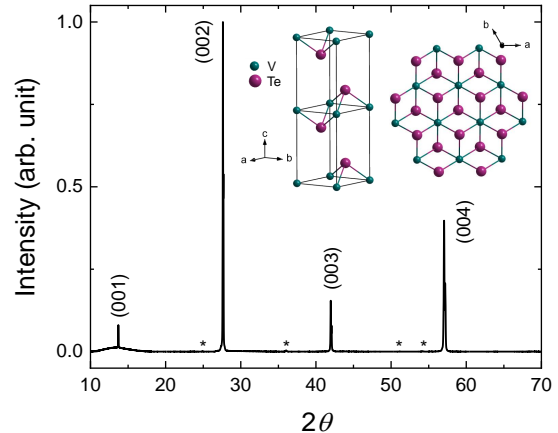


FIG. 1. (color online) X-ray diffraction patterns of $1T$ - VTe_2 single crystals. Asterisks mark peaks that do not belong to the trigonal phase. Inset: Schematic atomic structure of $1T$ - VTe_2 . Olive and purple circles represent V and Te atoms, respectively.

atoms (olive circles) located at the center of the octahedra formed by Te atoms (purple circles), as shown in the inset of Fig. 1. The V-Te layers are stacked along the c -axis by the van der Waals-like forces. As suggested by the transport and magnetic properties shown below, there is no additional structural transition down to 1.3 K. Sharp $(00l)$ Bragg peaks can be observed and yield a lattice constant $c = 6.456$ Å, which is similar to those of $1T$ - $V_{0.7}Ti_{0.3}Te_2$ single crystals [18] and $1T$ - VTe_2 nanoplates [22]. For single crystals made by the vapor transport method, the resulting CDW state leads to a monoclinic structure with $c = 9.069$ Å [17, 20]. As marked by asterisks in Fig. 1, a very small amount of unknown impurity phases has been identified. It corresponds to less than 2% of the sample volume and does not impact our studies or conclusions presented in the paper. The EDX analysis performed at different locations on the crystal surface of $1T$ - VTe_2 yields a V:Te composition close to $(1.01 \pm 0.03) : 2$.

B. Resistivity and magnetic susceptibility

The temperature dependence of the electrical resistivity $\rho(T)$ is illustrated in Fig. 2(a). At 300 K, the value of ρ is about 172.5 $\mu\Omega$ cm, close to that of $V_{0.7}Ti_{0.3}Te_2$ single crystals [18] while about an order of magnitude smaller than that of VTe_2 nanoplates [22]. In contrast to the CDW transition observed in $\rho(T)$ of $V_{1-x}Ti_xTe_2$ single crystals [18], no signature for a structural transition is found down to 2 K in VTe_2 single crystals. The $\rho(T)$ decreases from room temperature to a minimum value near 16 K. Rather than saturating at low temperatures, as expected for simple metals, the resistivity displays an in-

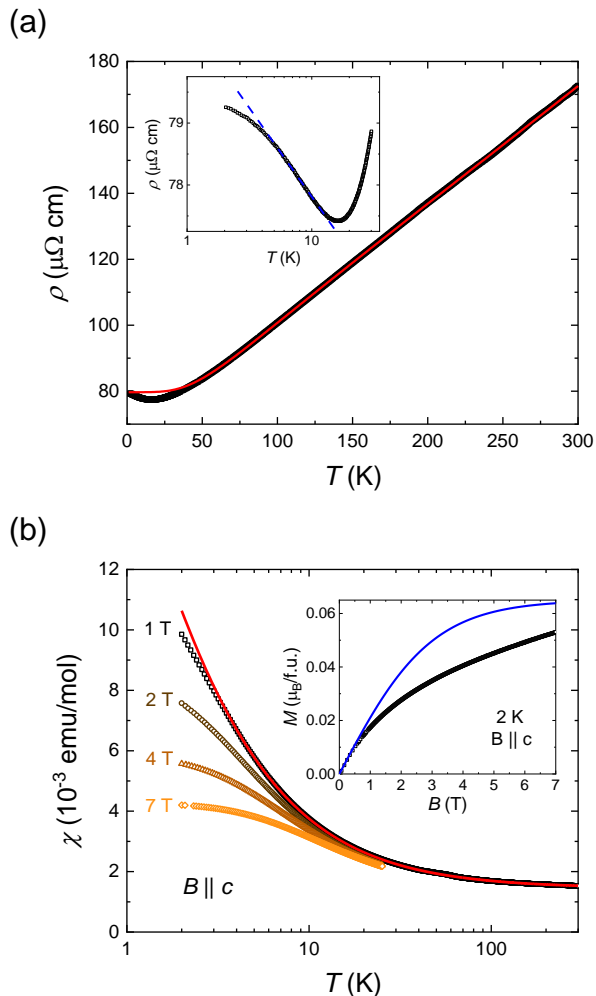


FIG. 2. (color online) (a) Temperature dependence of the in-plane electrical resistivity of VTe₂. Red curve is the fitting result of Eq. 1. Inset: An enlarged view of low temperatures in semi-log plots. Blue dashed line is a guide for the eye and shows a $-\ln T$ dependence. (b) Semi-log plots of the temperature dependence of the magnetic susceptibility of VTe₂, measured under several magnetic fields applied along the c -axis. Red line is the Curie-Weiss fit in the temperature range from 5 - 300 K at 1 T. Inset: Magnetic field dependence of the magnetization measured at 2 K. Blue line is calculated $M(B)$ using the Brillouin function Eq. (4).

crease with decreasing temperature below the minimum. The inset of Fig. 2(a) shows the low-temperature behavior on semi-log plots. The logarithmic increase below 16 K is characteristic of Kondo systems and it is due to a contribution from the conduction electron-magnetic impurity interaction [24]. Moreover, there is a divergence from the logarithmic increase below 5 K, mainly due to the spin-compensated state or the Ruderman-Kittel-Kasuya-Yosida (RKKY) interactions between magnetic impurities [34, 35]. The residual-resistivity ratio, defined as $\rho(300 \text{ K})/\rho(16 \text{ K})$, is relatively small and estimated to be only 2.2 in VTe₂ single crystals. This is consistent

with the presence of small amounts of impurities in the Kondo system. Therefore, the measured resistivity is the sum of the typical electron-phonon and electron-electron interactions, and the spin scattering of the conduction electrons by the magnetic impurity characteristic of the Kondo effect. First, we focus on the high-temperature behavior of the resistivity and consider the Kondo term ρ_K as a constant. As shown by the red line in Fig. 2(a), we fit $\rho(T)$ of 1T-VTe₂ in the temperature range 50 - 300 K to the formula

$$\rho(T) = \rho_0 + \rho_K + aT^2 + \rho_{\text{ph}}(T), \quad (1)$$

where $\rho_0 + \rho_K = 79.68 \mu\Omega \text{ cm}$ is the sum of the residual resistivity and the Kondo contribution, the aT^2 term represents the electron-electron interaction, and $\rho_{\text{ph}}(T)$ arises from electron-phonon interactions and is expressed by the Bloch-Grüneisen formula

$$\rho_{\text{ph}}(T) = \alpha \left(\frac{T}{\Theta_R} \right)^5 \int_0^{\frac{\Theta_R}{T}} \frac{x^5}{(e^x - 1)(1 - e^x)} dx. \quad (2)$$

In the model, α is a constant proportional to the electron-phonon coupling and Θ_R is the Debye temperature. The value $\Theta_R = 274 \text{ K}$ obtained from our electrical resistivity analysis is close to $\Theta_D = 267 \pm 20 \text{ K}$, as obtained from heat capacity measurement of VTe₂ polycrystals [36]. This approach fails to describe the low-temperature behavior of VTe₂ which can be well explained by including the Kondo effect. The analysis of the low-temperature part of $\rho(T)$ will be discussed below.

Figure 2(b) shows the temperature dependence of the magnetic susceptibility $\chi(T)$, measured under several values of the magnetic field along the c -axis. The susceptibility increases monotonically with decreasing temperature under 1 T. No magnetic order is observed down to 2 K. As shown by the red curve, the $\chi(T)$ data from 5 - 300 K could be well fitted to a modified Curie-Weiss formula

$$\chi(T) = \chi_0 - fT + \frac{C}{T - \theta}, \quad (3)$$

where $\chi_0 = 1.45 \times 10^{-3} \text{ emu/mol}$ is the Pauli susceptibility of conduction electrons in the host VTe₂. In general, the Pauli susceptibility of a metallic sample is temperature independent. However, in our case, a phenomenological fitting term $-fT$ with $f = 2.79 \times 10^{-7} \text{ emu}/(\text{mol K})$ needs to be added. The temperature-dependent Pauli susceptibility might be due to the change of relative sizes of the Fermi surface and Brillouin zones, where the crystal contract anisotropically with decreasing temperature. For instance, such behavior has been observed in α -U single crystals [37]. Similar linear temperature dependence for χ has been observed in the sister compound NiTe₂ [38], in which spin-polarized topological surface states were observed [39]. The third term is the Curie-Weiss susceptibility coming from Kondo impurities. As shown in the main frame of Fig. 2(b), the deviation of

$\chi(T)$ below 4 K from the fitting is further indication of Kondo behavior. It demonstrates the Kondo screening of the magnetic moment on the impurity from the surrounding cloud of negatively polarized conduction electrons, combined with the possible onset of short range order, mediated by an RKKY interaction between the intercalated V impurities. As the temperature decreases, the magnetic moment of the Kondo impurity crossover from localized behavior at high temperatures, described by the Curie-Weiss law, to a fully compensated moment at low temperatures, where temperature-independent Pauli susceptibility is formed [40]. We obtain the values of the Curie constant $C = 0.0246$ emu K/mol and the Curie-Weiss temperature $\theta = -0.676$ K. According to the EDX analysis, there are no other magnetic elements in the sample. Furthermore, layered compounds are easily intercalated with metallic guests due to their low-dimensional structures [7]. Thus, we assume that the intercalated V ions are indeed the magnetic impurities in the VTe_2 sample. Taking the spin of the localized V^{4+} ($S = 1/2$) into account, the theoretical magnetic moment of each scattering center is $\mu_V = g\sqrt{S(S+1)}\mu_B = 1.73\mu_B$, where $g = 2$ assuming quenched orbital contribution. Using the effective moment of the sample $\mu_{\text{eff}} \approx \sqrt{8C} = 0.443\mu_B/\text{f.u.}$, we estimate that the molar fraction of intercalated V ions is $N_1 = \mu_{\text{eff}}^2/\mu_V^2 = 0.066$. As shown in Fig. 2(b), similar to VSe_2 [10], the deviation of the susceptibility with respect to the Curie-Weiss law is more significant at higher magnetic fields. Moreover, the decrease of the saturated susceptibility indicates a reduction in the compensated moment of the impurity by the magnetic field. The inset of Fig. 2(b) shows the magnetic field dependence of the magnetization at 2 K. The induced magnetization is only $0.05\mu_B$ at 2 K and 7 T. By taking account the N_1 value obtained above, the magnetization could be calculated using the Brillouin function $B_J(x)$ with $J = 1/2$ as

$$M_{\text{cal}} = N_1 g \mu_B B_J \left(\frac{g \mu_B J B}{k_B T} \right). \quad (4)$$

As shown by the blue line in Fig. 2(b), the $M_{\text{cal}}(B)$ curve is compared to the measured data. The deviation above 0.3 T is mainly related to the splitting of the Kondo resonance under magnetic fields.

C. Magnetoresistivity

To further evaluate the magnetic Kondo impurity, we systematically measured the magnetic field dependence of MR, $\Delta\rho/\rho(0) = [\rho(B) - \rho(0)]/\rho(0) \times 100\%$ along the c -axis at different temperatures. The results are presented in the inset of Fig. 3(a). At 25 K, the negative MR(B) shows a convex shape in the entire field range. In contrast, the nonlinear MR at 2 K slightly bends upwards under high fields and reaches -3.7% at 14 T. The negative MR has been derived by Yosida from the first-order

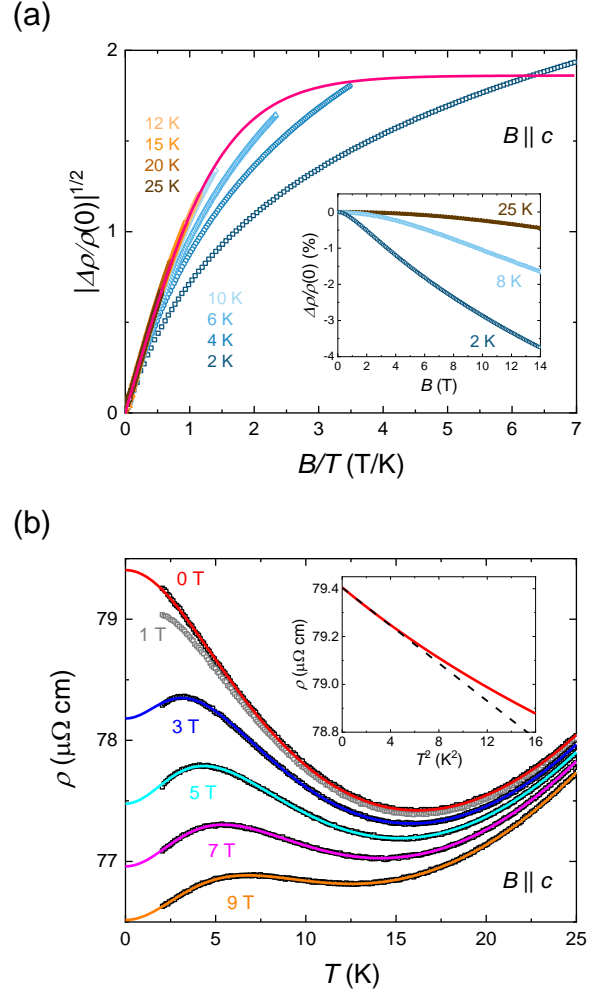


FIG. 3. (color online) (a) Square root of $|\Delta\rho/\rho(0)|$ as a function of B/T measured at various temperatures. Pink line is the Brillouin function with a scaled magnitude. Inset: Magnetic field dependence of the MR at different temperatures. (b) Temperature dependence of the resistivity under different magnetic fields. Solid lines are fits to the modified Hamann expression Eq. (6) and (8). Inset: An enlarged view of the fitting curve under zero magnetic field is shown by the red line. Black dashed line is a guide for the eye and shows a $-T^2$ dependence.

perturbation of the s - d exchange interaction [41]. If magnetic moments existed, the magnitude of the negative MR should be proportional to the square of the impurity magnetization, for $T > T_K$ and in the low B/T limit [42]. Accordingly, we plot $|\Delta\rho/\rho(0)|$ as a function of B/T for different temperatures in Fig. 3(a). It is clear that the negative MR above 12 K collapses and can be scaled by the Brillouin function ($J = 1/2$)

$$\left| \frac{\Delta\rho}{\rho(0)} \right|^{\frac{1}{2}} = \lambda B_J \left(\frac{g \mu_B J B}{k_B T} \right), \quad (5)$$

where λ is a scaling constant. These results strongly support the scenario of the localized V impurity with $S = 1/2$. The gradual deviation from the scaling function below 12 K indicates the screening conduction electrons, which is a scale determined by many-body interactions. Thus, we obtain the Kondo temperature $T_K = 12$ K, where the Kondo resonance is gradually formed.

In order to analyze the Kondo effect in VTe_2 in greater detail, we focus on the low-temperature behavior of the resistivity in this system. Fig. 3(b) shows the temperature dependence of resistivity from 2 to 25 K and under different magnetic fields applied along the c -axis. Since the phonon contribution is small at low temperatures and doesn't change under magnetic fields, we analyze the low-temperature data by taking into account the Fermi liquid behavior and the contribution from the Kondo scattering only. The Hamann expression, yielding a new solution for the s - d exchange model, is mostly used for analyzing the Kondo effect in the low-temperature electrical resistivity. It was reduced from Nagaoka's self-consistent equations to a single nonlinear integral equation [43]. However, its applicability is limited to temperatures $T \geq T_K$. For $T < T_K$, the Hamann expression gives low values for the impurity spin S due to inadequacies in the Nagaoka's approximation [44]. To account for this issue, we replace the variable T with $T_{\text{eff}} = \sqrt{T^2 + T_W^2}$, where $k_B T_W$ is the effective RKKY interactions [34, 45]. As demonstrated by the red line, $\rho(T)$ under zero field can be analyzed by the formula

$$\rho(T) = \rho_0 + aT^2 + \rho_H(T_{\text{eff}}), \quad (6)$$

where ρ_0 is the residual resistivity, $\rho_H(T_{\text{eff}})$ is the modified Hamann expression [34, 43, 45], which leads to the crossover region and to saturation at low temperatures, and is given by

$$\rho_H(T_{\text{eff}}) = \rho_K \left[1 - \frac{\ln(T_{\text{eff}}/T_K)}{\sqrt{\ln^2(T_{\text{eff}}/T_K) + \pi^2 S(S+1)}} \right], \quad (7)$$

where ρ_K is a temperature-independent constant, $T_W = 5.18$ K is related to the average RKKY interaction strength between V impurities and its value is close to the deviation temperature of the logarithmic increase. According to the above MR analysis, the spin of the magnetic impurities S and the Kondo temperature T_K are fixed to $1/2$ and 12 K, respectively. As shown in the inset of Fig. 3(b), in the Kondo regime at $T \ll T_K$, the red fitting curve exhibits the $-T^2$ dependence below 2 K, characteristics of single-impurity Kondo effect and Nagaoka theory [34, 44, 46, 47]. Thus, the modified Hamann expression gives a phenomenologically satisfactory description of the logarithmic increase with decreasing temperature in a small range below T_K and the $-T^2$ behavior at $T \ll T_K$ in $\rho(T)$ [48].

Because the system shows negative MR, it is expected that the upturn of $\rho(T, B)$ is suppressed with increasing magnetic fields. Moreover, the splitting of the Kondo

resonance under applied magnetic fields correlates with the electrical transport property, in which $\rho(T, B)$ shows an extra increase with decreasing temperature below T_K . As shown in Fig. 3(b), a finite temperature peak is observed when the applied magnetic field is larger than 3 T. With increasing magnetic field, the peak becomes broader and shifts to higher temperatures. Motivated by previous theoretical calculations [42] and experimental analysis of $Ce_xLa_{1-x}Al_2$ alloys [30], an impurity spin polarization function $[1-L^2(x)]$ is added to the modified Hamann expression in Eq. (7) for the analysis of $\rho(T, B)$. Not only magnetic impurities interact with the conduction electrons below T_K , but also the relaxation time describing the Kondo resonance is different for up spins and down spins when a large enough magnetic field is applied [41]. Therefore, we use the Langevin function $L(x)$ instead of the Brillouin function $B_J(x)$ for the analysis of $\rho(T, B)$ [30]. Furthermore, the variable B/T of the Langevin function is replaced by B/T_{eff}

$$\rho_H(T_{\text{eff}}, B) = \rho_K \left[1 - \frac{\ln(T_{\text{eff}}/T_K)}{\sqrt{\ln^2(T_{\text{eff}}/T_K) + \pi^2 S(S+1)}} \right] \cdot \left\{ 1 - L^2 \left[\frac{\mu B}{k_B T_{\text{eff}}} \right] \right\}, \quad (8)$$

where μ is the effective magnetic moment of the vanadium impurity. The values for T_K and S , as fixed in the fitting of the zero-field resistivity, are left unchanged. As shown in Fig. 3(b), the change of MR at 1 T is relatively small. This indicates that magnetic field might not be strong enough to split the Kondo resonance at finite temperatures [29]. Also, for a reliable analysis of the result by Eq.(8) at low magnetic fields, measurements at lower temperatures are required (below 2 K). All fitting parameters are listed in Table I. The term $\rho_0 + \rho_K$ gradually decreases with an increasing magnetic field, which is consistent with the negative MR. The reduction of μ indicates that the impurity gradually loses its magnetic character under magnetic fields. This is also reflected in the magnetic susceptibility measurements in Fig. 2(b). The 3d vanadium impurity is unique, because its magnetic moment varies from 0 in bulk V and clusters of V atoms, via $3/5 \mu_B$ in the atomic model, to a maximum of $3 \mu_B$ in the d resonance model [49]. In VSe_2 , previous work suggests that the intercalated V ion produces a net paramagnetic moment of $2.5 \mu_B$ [10, 50]. A related point to consider is that a magnetic moment as large as $6.5 \mu_B$ was reported for V impurities in thin films of Na host, indicating a polarization of the host [49]. In the last section, we used the magnetic moment of quenched V^{4+} ions to estimate the molar fraction of V impurities. Here, using $\mu(3 \text{ T}) = 2.436 \mu_B$ from the Langevin function fit, the molar fraction is estimated to be $N_2 = \mu_{\text{eff}}^2/\mu^2 = 0.033$, which is closer to the EDX result for the deviation from stoichiometry $N = 0.01 \pm 0.03$.

The characteristic peaks observed under magnetic fields are mostly observed in dilute magnetic alloys [30] and strongly interacting quantum dots [51]. A detailed

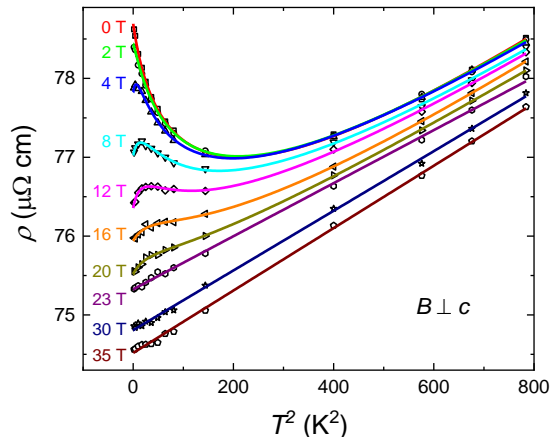


FIG. 4. (color online) Resistivity as a function of T^2 measured under different magnetic fields applied perpendicularly to the c -axis. Discrete data points were determined from the measurements by sweeping the magnetic field at a fixed temperature. Solid lines are fits at different magnetic fields (see text).

NRG calculation has previously been done for the $\rho(T, B)$ of dilute magnetic alloy $\text{Ce}_x\text{La}_{1-x}\text{Al}_2$, $x = 0.0063$ [29]. Comparing with the NRG calculation, our modified Hamann expression demonstrates a valid extension of $\rho(T, B)$ to $T \ll T_K$. It is worth mentioning that, in heavy fermion $\text{Ce}_x\text{La}_{1-x}\text{Cu}_6$, a continuous crossover from the single impurity Kondo system to the coherent Kondo lattice occurs with increasing the Ce impurity concentration [52]. The resistivity for the concentrated Ce samples ($x > 0.5$) has maximum below T_K , which drops steeply with decreasing temperature. This type of maximum in $\rho(T)$ under zero magnetic field, observed in Kondo lattice materials, is due to the RKKY interactions between a periodic arrangement of Kondo ions.

To systematically study the characteristic peaks in $\rho(T, B)$ of $1T\text{-VTe}_2$ single crystals, further investigation of the magnetic-field-induced splitting of Kondo resonance is provided by the MR measurements performed under very high magnetic fields up to 35 T (the magnetic field is applied perpendicular to the c -axis). At 1.3 K, the negative MR reaches -5.2% at 35 T. Figure 4 shows the resistivity versus T^2 measured under different magnetic fields. As can be seen, the peak in $\rho(T, B)$ is clearly visible at lower fields, but flattens out with increasing magnetic fields. For magnetic fields below 23 T, the data were analyzed by using the modified Hamann expression Eq. (6) and (8). At high magnetic fields, the anomaly is no longer detectable, and the temperature dependence of the resistivity above 23 T could be fitted to $\rho(T) = \rho_0 + \rho_K + aT^2$. It is clear that the negative MR does not saturate after the anomaly is suppressed. This might indicate that higher magnetic fields are required to fully suppress the Kondo effect. The fitting

TABLE I. Parameters obtained from analysis of $\rho(B, T)$ in Fig. 3 and Fig. 4 where $S = 1/2$ and $T_K = 12$ K are fixed.

B (T)	$\rho_0 + \rho_K$ ($\mu\Omega$ cm)	a	ρ_K ($\mu\Omega$ cm)	T_W (K)	μ (μ_B)
$B \parallel c$					
0	77.1371	0.00455	7.2712	4.897	
3	77.0111	0.0045	6.9683	3.4324	2.4362
5	76.9279	0.00449	6.7993	3.8448	1.8888
7	76.8132	0.00447	6.5191	4.4409	1.6457
9	76.6433	0.00439	5.9707	4.923	1.4798
$B \perp c$					
0	76.497	0.005	6.3749	4.4231	
2	76.5056	0.00488	6.1447	3.7431	2.0637
4	76.469	0.00467	5.5658	2.9452	1.3954
8	76.4011	0.00457	5.3078	3.9616	1.0938
12	76.1831	0.00439	4.2895	4.1695	0.8927
16	76.0906	0.00464	4.7916	6.4127	0.9462
20	75.6252	0.00406	2.2738	5.3276	0.7311
23	75.3252	0.00337			
30	74.8073	0.00378			
35	74.5179	0.00396			

parameters are included in Table I. It is worth noting that the Fermi liquid behavior (the a coefficient, in particular) at high temperatures $T > T_K$ and zero magnetic field is roughly the same as the Fermi liquid slope at low temperatures and 35 T (see Table I). As shown by the NRG calculations [29], the magnetic field splits and suppress the Kondo resonance which is due to the interaction between the magnetic impurity and the conduction electrons. Our results demonstrate that the Kondo effect is gradually suppressed and the system shows a crossover to the Fermi liquid state under high magnetic fields.

D. Hall effect

Figure 5(a) shows the magnetic field dependence of the Hall resistivity $\rho_{yx}(B)$ measured at different temperatures up to 10 T. The red line is a linear fit of $\rho_{yx}(B)$ from 0 to 5 T, characteristic of the ordinary Hall effect. By having a scrutiny to $\rho_{yx}(B)$, the deviation from the linearity occurs at high magnetic fields below T_K , which is consistent with the splitting of the Kondo resonance by the magnetic field. The Hall coefficient, $R_H = \rho_{yx}/B$ at 5 T, is plotted versus temperature in Fig. 5(b). The positive R_H over the whole temperature range reveals that the electrical conduction is dominated by hole-type charge carriers. In contrast to the electron-type carriers in the VTe_2 nanoplates [22], our results are consistent with the hole-like bands in the monolayer $1T\text{-VTe}_2$ [13] and the result of recent angle-resolved photoemission spectroscopy measurements of $1T\text{-V}_{1-x}\text{Ti}_x\text{Te}_2$, which characterize the circular and triangular hole-type

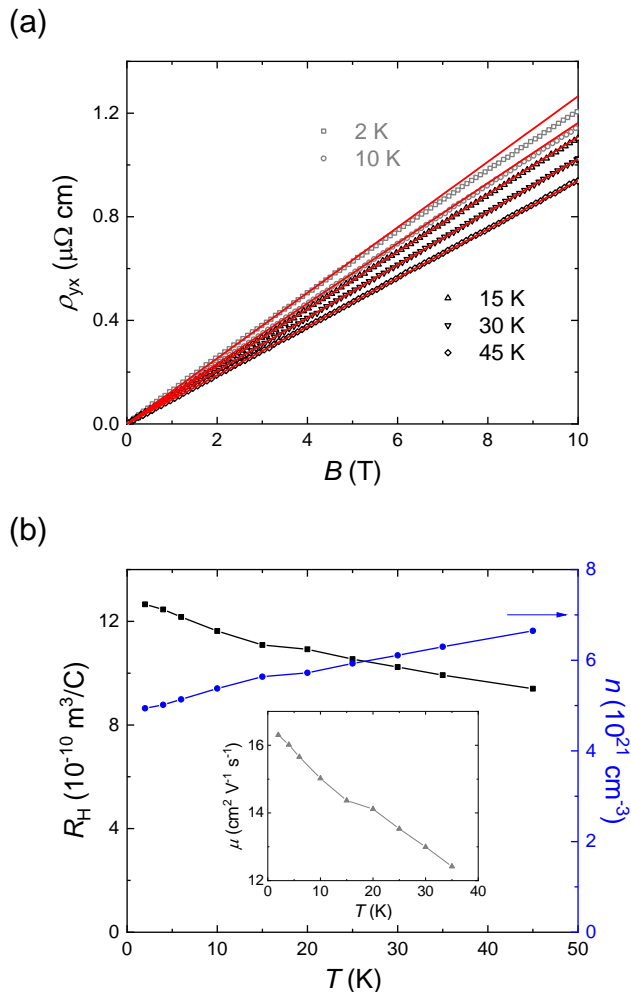


FIG. 5. (color online) (a) Magnetic field dependence of Hall resistivity at various temperatures of VTe₂. Red lines are linear fit from 0 to 5 T. (b) Temperature dependence of the Hall coefficient and effective charge carrier density. Inset: Hall mobility μ_H vs temperature at $B = 5 \text{ T}$.

Fermi surfaces around Γ and K points, respectively [19]. As shown in Fig. 5(b), the R_H exhibits a temperature dependency that differs from the expected one band approximation in simple metals. This might indicate a complex electronic structure in VTe₂, where the bands have temperature-dependent carrier concentrations and mobilities. Furthermore, R_H increases with decreasing

temperature with an anomaly at $T \sim T_K$, which is characteristic for the Kondo effect [48]. The blue curve displays the temperature dependence of the effective charge-carrier density n , obtained by the formula $R_H = 1/ne$ (one band approximation). At 45 K, the estimated concentration of free electrons is $6.7 \times 10^{21} \text{ cm}^{-3}$. This value of n , due to the crude approximation that neglects the semimetallic character of the compound, can be considered as an upper limit of the real concentration in this material. The temperature dependence of the Hall mobility $\mu_H(T)$ calculated with the single-band scenario at 5 T is shown in the inset of Fig. 5(b). At 35 K, the value of μ_H is $12.42 \text{ cm}^2 \text{ V}^{-1} \text{ s}^{-1}$.

IV. CONCLUSIONS

In summary, we have successfully synthesized single crystals of 1T-VTe₂ and measured their detailed magnetic and magnetotransport properties at low temperatures and under high magnetic fields. The magnetic susceptibility, electrical resistivity, and Hall effect are systematically studied revealing the presence of the Kondo behavior in this material. From the negative MR measurements, we point out that the intercalated V may act as the Kondo impurities. The observation of a peak below T_K in $\rho(T, B)$ reflects the splitting of the Kondo resonance. The analysis by using the modified Hamann expression is in good agreement with the experimental results. Furthermore, we directly show that the Kondo behavior is suppressed by strong magnetic fields, and for the fields above 23 T the bulk VTe₂ material behaves as an ordinary Fermi liquid system.

V. ACKNOWLEDGMENTS

This work is supported by the National Natural Science Foundation of China (Grant No. A0402/11534005 and A0402/11674164). X.D. acknowledges support from INLs LDRD program (19P43-013FP). K.G. acknowledges support from the US DOE BES Energy Frontier Research Centre "Thermal Energy Transport under Irradiation" (TETI). L.B. is supported by DOE-BES through award DE-SC0002613. The National High Magnetic Field Laboratory is supported by the National Science Foundation Cooperative Agreement No. DMR-1644779 and the State of Florida.

- [1] J. Wilson and A. Yoffe, The transition metal dichalcogenides discussion and interpretation of the observed optical, electrical and structural properties, *Advances in Physics* **18**, 193 (1969).
 [2] Q. H. Wang, K. Kalantar-Zadeh, A. Kis, J. N. Coleman, and M. S. Strano, *Electronics and optoelectronics*

of two-dimensional transition metal dichalcogenides, *Nature nano.* **7**, 699 (2012).

- [3] M. Chhowalla, H. S. Shin, G. Eda, L.-J. Li, K. P. Loh, and H. Zhang, The chemistry of two-dimensional layered transition metal dichalcogenide nanosheets, *Nature chem.* **5**, 263 (2013).

- [4] R. Morris, R. Coleman, and R. Bhandari, Superconductivity and magnetoresistance in NbSe_2 , *Phys. Rev. B* **5**, 895 (1972).
- [5] J. Wilson, F. D. Salvo, and S. Mahajan, Charge-density waves and superlattices in the metallic layered transition metal dichalcogenides, *Advances in Physics* **24**, 117 (1975), <https://doi.org/10.1080/00018737500101391>.
- [6] M. N. Ali, J. Xiong, S. Flynn, J. Tao, Q. D. Gibson, L. M. Schoop, T. Liang, N. Haldolaarachchige, M. Hirschberger, N. Ong, *et al.*, Large, non-saturating magnetoresistance in WTe_2 , *Nature* **514**, 205 (2014).
- [7] M. Whittingham, Chemistry of intercalation compounds: Metal guests in chalcogenide hosts, *Progress in Solid State Chemistry* **12**, 41 (1978).
- [8] E. Morosan, H. W. Zandbergen, B. S. Dennis, J. W. G. Bos, Y. Onose, T. Klimczuk, A. P. Ramirez, N. P. Ong, and R. J. Cava, Strong room-temperature ferromagnetism in VSe_2 monolayers on van der waals substrates, *Nature Physics* **2**, 544 (2006).
- [9] M. Sasaki, A. Ohnishi, T. Kikuchi, M. Kitaura, K.-S. Kim, and H.-J. Kim, Interplay between the kondo effect and randomness: Griffiths phase in $M_x\text{Te}_2$ ($m = \text{Co}, \text{Ni}$, and Fe) single crystals, *Phys. Rev. B* **82**, 224416 (2010).
- [10] S. Barua, M. C. Hatnean, M. R. Lees, and G. Balakrishnan, Signatures of the kondo effect in VSe_2 , *Scientific Reports* **7**, 10964 (2017).
- [11] M. Bonilla, S. Kolekar, Y. Ma, H. C. Diaz, V. Kalappattil, R. Das, T. Eggers, H. R. Gutierrez, M.-H. Phan, and M. Batzill, Strong room-temperature ferromagnetism in VSe_2 monolayers on van der waals substrates, *Nature Nanotechnology* **13**, 289 (2018).
- [12] P. M. Coelho, K. Lasek, K. Nguyen Cong, J. Li, W. Niu, W. Liu, I. I. Oleynik, and M. Batzill, Monolayer modification of VTe_2 and its charge density wave, *The Journal of Physical Chemistry Letters* **10**, 4987 (2019), pMID: 31411022, <https://doi.org/10.1021/acs.jpcclett.9b01949>.
- [13] K. Sugawara, Y. Nakata, K. Fujii, K. Nakayama, S. Souma, T. Takahashi, and T. Sato, Monolayer VTe_2 : Incommensurate fermi surface nesting and suppression of charge density waves, *Phys. Rev. B* **99**, 241404(R) (2019).
- [14] Y. Wang, J. Ren, J. Li, Y. Wang, H. Peng, P. Yu, W. Duan, and S. Zhou, Evidence of charge density wave with anisotropic gap in a monolayer VTe_2 film, *Phys. Rev. B* **100**, 241404(R) (2019).
- [15] Q. Wu, Z. Wang, Y. Guo, F. Yang, and C. Gao, Orbital-collaborative charge density waves in monolayer VTe_2 , *Phys. Rev. B* **101**, 205105 (2020).
- [16] T. Ohtani, K. Hayashi, M. Nakahira, and H. Nozaki, Phase transition in $\text{V}_{1+x}\text{Te}_2$ ($0.04 \leq x \leq 0.11$), *Solid State Comm.* **40**, 629 (1981).
- [17] K. Bronsema, G. Bus, and G. Wiegers, The crystal structure of vanadium ditelluride, $\text{V}_{1+x}\text{Te}_2$, *Journal of Solid State Chemistry* **53**, 415 (1984).
- [18] M. Kamitani and S. Tatsuya, Single crystal growth of Ti doped VTe_2 and the elucidation of the electronic structure by ARPES, Available at http://www.ap.t.u-tokyo.ac.jp/merit/en/training/pdf/report/kamitani_sonobe.pdf (2015).
- [19] N. Mitsuishi, Y. Sugita, M. S. Bahramy, M. Kamitani, T. Sonobe, M. Sakano, T. Shimojima, H. Takahashi, H. Sakai, K. Horiba, H. Kumigashira, K. Taguchi, K. Miyamoto, T. Okuda, S. Ishiwata, Y. Motome, and K. Ishizaka, Switching of band inversion and topological surface states by charge density wave, *Nature Communications* **11**, 2466 (2020).
- [20] K. S. Nikonov, M. N. Brekhovskikh, A. V. Egorysheva, T. K. Menshchikova, and V. A. Fedorov, Chemical vapor transport growth of vanadium(IV) selenide and vanadium(IV) telluride single crystals, *Inorganic Materials* **53**, 1126 (2017).
- [21] X. Ding, *Transport research on $K_x\text{Fe}_{2-y}\text{Se}_2$ and VTe_2 single crystals*, Ph.D. thesis, Nanjing University (2015).
- [22] H. Liu, Y. Xue, J.-A. Shi, R. A. Guzman, P. Zhang, Z. Zhou, Y. He, C. Bian, L. Wu, R. Ma, J. Chen, J. Yan, H. Yang, C.-M. Shen, W. Zhou, L. Bao, and H.-J. Gao, Observation of the kondo effect in multilayer single-crystalline VTe_2 nanoplates, *Nano Letters* **19**, 8572 (2019).
- [23] W. Meissner and B. Vogit, *Ann. Phys.* **399**, 761 (1930).
- [24] J. Kondo, Resistance minimum in dilute magnetic alloys, *Prog. of Theo. Phys.* **32**, 37 (1964).
- [25] A. Zhao, Q. Li, L. Chen, H. Xiang, W. Wang, S. Pan, B. Wang, X. Xiao, J. Yang, J. G. Hou, and Q. Zhu, Controlling the kondo effect of an adsorbed magnetic ion through its chemical bonding, *Science* **309**, 1542 (2005).
- [26] M. R. Calvo, J. Fernández-Rossier, J. J. Palacios, D. Jacob, D. Natelson, and C. Untiedt, The kondo effect in ferromagnetic atomic contacts, *Nature* **458**, 1150 (2009).
- [27] A. A. Abrikosov and A. A. Migdal, On the theory of the kondo effect, *Journal of Low Temperature Physics* **3**, 519 (1970).
- [28] K. G. Wilson, The renormalization group: Critical phenomena and the kondo problem, *Rev. Mod. Phys.* **47**, 773 (1975).
- [29] T. Costi, Kondo effect in a magnetic field and the magnetoresistivity of kondo alloys, *Phys. Rev. Lett.* **85**, 1504 (2000).
- [30] W. Felsch and K. Winzer, Magnetoresistivity of (1a, c) Al_2 alloys, *Solid State Comm.* **13**, 569 (1973).
- [31] C. van Bruggen and C. Haas, Magnetic susceptibility and electrical properties of VSe_2 single crystals, *Solid State Communications* **20**, 251 (1976).
- [32] M. Bayard and M. Sienko, Anomalous electrical and magnetic properties of vanadium diselenide, *Journal of Solid State Chemistry* **19**, 325 (1976).
- [33] D. Murphy, F. Di Salvo, and J. Carides, Vanadium disulfide: Metal substitution and lithium intercalation, *Journal of Solid State Chemistry* **29**, 339 (1979).
- [34] J. Kästner and E. F. Wassermann, Kondo effect and impurity interactions in the resistivity of dilute ZnMn alloys, *Journal of Low Temperature Physics* **29**, 411 (1977).
- [35] V. K. C. Liang and C. C. Tsuei, Kondo effect in an amorphous $\text{Ni}_{41}\text{Pd}_{41}\text{B}_{18}$ alloy containing Cr, *Phys. Rev. B* **7**, 3215 (1973).
- [36] A. A. Vinokurov, A. V. Tyurin, A. L. Emelina, K. S. Gavrichev, and V. P. Zlomanov, Thermodynamic properties of VTe_2 , *Inorganic Materials* **45**, 480 (2009).
- [37] J. W. Ross and D. J. Lam, Magnetic susceptibility of single-crystal alpha-uranium, *Phys. Rev.* **165**, 617 (1968).
- [38] Q. Mao, Y. Zhang, Q. Chen, R. Li, X. Geng, J. Yang, H. Hao, and M. Fang, Metallicity and paramagnetism of single-crystalline nite and nite₂, *physica status solidi (b)* **257**, 1900224 (2020), <https://onlinelibrary.wiley.com/doi/pdf/10.1002/pssb.201900224>.
- [39] B. Ghosh, D. Mondal, C.-N. Kuo, C. S. Lue, J. Nayak, J. Fujii, I. Vobornik, A. Politano, and A. Agarwal, Observation of bulk states and spin-polarized topological

- surface states in transition metal dichalcogenide dirac semimetal candidate NiTe_2 , *Phys. Rev. B* **100**, 195134 (2019).
- [40] K. Park, L. S. Wu, Y. Janssen, M. S. Kim, C. Marques, and M. C. Aronson, Field-tuned fermi liquid in quantum critical $\text{YFe}_2\text{Al}_3\text{O}$, *Phys. Rev. B* **84**, 094425 (2011).
- [41] K. Yosida, Anomalous electrical resistivity and magnetoresistance due to an s-d interaction in Cu-Mn alloys, *Phys. Rev.* **107**, 396 (1957).
- [42] M.-T. Béal-Monod and R. A. Weiner, Negative magnetoresistivity in dilute alloys, *Phys. Rev.* **170**, 552 (1968).
- [43] D. R. Hamann, New solution for exchange scattering in dilute alloys, *Phys. Rev.* **158**, 570 (1967).
- [44] Y. Nagaoka, Self-consistent treatment of kondo's effect in dilute alloys, *Phys. Rev.* **138**, A1112 (1965).
- [45] K. Fischer, Effect of ordinary scattering on the resistivity anomaly due to magnetic impurities, *Journal of Physics and Chemistry of Solids* **29**, 1227 (1968).
- [46] P. Nozières, A "fermi-liquid" description of the kondo problem at low temperatures, *Journal of Low Temperature Physics* **17**, 31 (1974).
- [47] A. Gauzzi, H. Moutaabbid, Y. Klein, G. Louprias, and V. Hardy, Fermi- to non-fermi-liquid crossover and kondo behavior in two-dimensional $(\text{Cu}_2/3\text{V}_1/3)\text{V}_2\text{S}_4$, *Journal of Physics: Condensed Matter* **31**, 31LT01 (2019).
- [48] T. A. Costi, A. C. Hewson, and V. Zlatic, Transport coefficients of the anderson model via the numerical renormalization group, *Journal of Physics: Condensed Matter* **6**, 2519 (1994).
- [49] F. Song and G. Bergmann, Strongly enhanced magnetic moments of vanadium impurities in thin films of sodium and potassium, *Phys. Rev. Lett.* **88**, 167202 (2002).
- [50] A. H. Thompson and B. G. Silbernagel, Correlated magnetic and transport properties in the charge-density-wave states of VSe_2 , *Phys. Rev. B* **19**, 3420 (1979).
- [51] D. Goldhaber-Gordon, J. Göres, M. A. Kastner, H. Shtrikman, D. Mahalu, and U. Meirav, From the kondo regime to the mixed-valence regime in a single-electron transistor, *Phys. Rev. Lett.* **81**, 5225 (1998).
- [52] Y. Ōnuki and T. Komatsubara, Heavy fermion state in CeCu_6 , *Journal of Magnetism and Magnetic Materials* **63-64**, 281 (1987).